



Novel polychrome staining distinguishing osteochondral tissue and bone cells in decalcified paraffin sections

Tepei Nakamura^{1,2} · Kanako Sumi¹ · Erika Tsuji¹ · Marina Hosotani³ · Takashi Namba² · Osamu Ichii^{2,4} · Takao Irie^{5,6} · Ken-ichi Nagasaki⁷ · Yasuhiro Kon² · Takashi Mishima¹ · Tomoji Yoshiyasu¹

Received: 28 April 2021 / Accepted: 26 July 2021 / Published online: 19 August 2021
© The Author(s), under exclusive licence to Springer-Verlag GmbH Germany, part of Springer Nature 2021

Abstract

The bone is a dynamic and metabolically active organ in which growth and resorption of the osteochondral matrix is orchestrated by osteoblasts and osteoclasts. For decalcified paraffin-embedded specimens, decalcifying agents alter the staining intensity, and excess decalcification interferes with bone staining. Robust bone staining methods independent of the decalcification conditions and animal species are lacking. In this study, we have developed a novel polychrome staining method, named JFRL staining, which stains the components of osteochondral tissue in different colors. With this staining we could visualize the hyaline cartilage as blue by alcian blue, osteoid as red by picosirius red, and mineralized bone as green by picro-light green SF or picro-naphthol green B and easily distinguished osteoblasts, osteocytes, and osteoclasts. In mineralized bone, this staining revealed the obvious lamellar structures and woven bone. Notably, this staining was independent of the decalcification conditions and experimental animal species examined. To verify the usefulness of JFRL staining, we observed cotton rat tail which has shorter length and shows a false autotomy. The caudal vertebrae were normally developed via endochondral ossification without a fracture plane. At 6 months of age, the number of chondrocytes declined and the hypertrophic zone was absent at the epiphyseal plate, which might reflect the shorter tail. In conclusion, JFRL staining is the first method to simultaneously distinguish osteochondral matrix and bone cells in one section regardless of decalcifying conditions. This robust staining will provide new information for a wide number of biomedical fields, including bone development, physiology, and pathology.

Keywords Osteoid · Mineralized bone · Cartilage · Bone cells · Osteochondral staining

Introduction

Bone is a dynamic and metabolically active organ in which simultaneous growth and resorption of the bone matrix is orchestrated by osteoblasts and osteoclasts under hormonal

regulation. The bone is formed via two pathways: intramembranous ossification and endochondral ossification (Gilbert 2000). During development, flat bones are formed by intramembranous ossification, where osteoblasts differentiate directly from mesenchymal stem cells to form the bone matrix. In

✉ Tepei Nakamura
nakamura@jfrl.or.jp

¹ Department of Biological Safety Research, Chitose Laboratory, Japan Food Research Laboratories, Hokkaido, Chitose 066-0052, Japan

² Laboratory of Anatomy, Department of Basic Veterinary Sciences, Faculty of Veterinary Medicine, Hokkaido University, Hokkaido, Sapporo 060-0818, Japan

³ Laboratory of Veterinary Anatomy, Department of Veterinary Medicine, School of Veterinary Medicine, Rakuno Gakuen University, Ebetsu, Hokkaido 069-8501, Japan

⁴ Laboratory of Agrobiomedical Science, Faculty of Agriculture, Hokkaido University, Sapporo, Hokkaido 060-0818, Japan

⁵ Medical Zoology Group, Department of Infectious Diseases, Hokkaido Institute of Public Health, Sapporo, Hokkaido 060-0818, Japan

⁶ Laboratory of Veterinary Parasitology, Faculty of Agriculture, University of Miyazaki, Miyazaki 889-2192, Japan

⁷ Department of Biological Safety Research, Tama Laboratory, Japan Food Research Laboratories, Tokyo, Tama 206-0025, Japan

contrast, long bones are formed by endochondral ossification, where chondrocytes differentiate from mesenchymal stem cells to produce cartilage, and the mineralized cartilage is replaced by the bone matrix (Gilbert 2000). After birth, both processes remain, and the latter is found at the epiphyseal plate of the long bones and temporarily during bone healing after fracture (Moreira et al. 2019; Bahney et al. 2019). The epiphyseal plate consists of reserve (resting), proliferative, and hypertrophic zones depending on the stages of chondrocyte differentiation (Roach et al. 2003). The bone matrix is composed of two elements—the osteoid bone and calcified bone. Osteoid, the newly formed unmineralized bone matrix composed of type I collagen, is produced by osteoblasts (Moreira et al. 2019). The osteoid becomes filled with calcium phosphate to form the mature form—calcified bone, and osteoblasts differentiate into mature form, osteocytes. The old or damaged calcified bone is removed by osteoclasts. Mineralized bone is morphologically visualized as two types. When the bone is formed rapidly during development and during fracture healing, it is not tightly packed and is called woven bone (Moreira et al. 2019). Woven bone is progressively replaced by mature lamellar bone (Moreira et al. 2019).

An imbalance between osteoblast-mediated bone formation and osteoclast-mediated resorption may lead to abnormal bone remodeling and bone disorders. Osteomalacia is exhibited by elevated osteoid formation due to delayed bone mineralization, whereas other disorders such as hypoparathyroidism increases mineralized bone due to excess mineralization (Kulak and Dempster 2010). Humans, companion animals, and laboratory animals all develop bone metabolic diseases, and diagnosis of these metabolic bone diseases requires a histomorphometric analysis. As mentioned above, bone homeostasis is tightly regulated by complex processes. It is important to simultaneously stain the osteochondral matrix and bone cells in bone development, physiology, and pathology using rapid, robust, and highly reproducible staining methods.

Several staining methods can be used to distinguish the different components of the bone matrix. For undecalcified specimens, Villanueva osteochrome bone stain, or Villanueva-Goldner staining are routinely used to distinguish between osteoid and calcified bone (Ueno 1985). Other bone staining techniques can also be applied to decalcified paraffin-embedded specimens. Pretreatment with cyanuric chloride followed by hematoxylin and eosin increases the staining intensity of the osteoid (Yoshiki 1973). Movat's pentachrome, Masson-Goldner's trichrome, or Ralis tetrachrome staining stains the osteoid and mineralized bone with different colors (Ralis and Watkins 1992; Rentsch et al. 2014). Before these staining procedures, the bone specimens are decalcified using inorganic acids, organic acids, or chelators such as hydrochloric acid, formic acid, or ethylene diamine tetra acetic acid (EDTA), respectively (Bogoevski et al. 2019). Among the different decalcification agents, treatment

with inorganic acid yields rapid decalcification, but has a high potential for tissue damage and also interferes with bone staining (Ralis and Watkins 1992; Bogoevski et al. 2019). To the best of our knowledge, no suitable staining is available for bone matrix with over-decalcification.

In this study, we have developed a novel polychrome staining method that simultaneously detects osteochondral tissues regardless of the decalcification method, and named it—Join of the Five dyes Revealing coLLagenous tissue (JFRL) staining. This staining also visualizes bone cells, such as osteoblasts, osteocytes, and osteoclasts unless the sections are over-decalcified. To clarify the usefulness of the JFRL staining, we examined the time-course changes of the caudal vertebrae in the cotton rats, *Sigmodon hispidus*. The cotton rat is a rodent, classified in the family Cricetidae and has been selected as a laboratory animal model in the field of infectious research because it can faithfully mimic human infectious diseases (Niewiesk and Prince 2002). The cotton rats have a relatively shorter tail and show false caudal autotomy characterized by loss of the tail sheath with the caudal vertebrae remaining (Faith et al. 1997; Hosotani et al. 2021). Although the fracture plane of the skin has been clarified (Hosotani et al. 2021), those of the caudal vertebrae have not yet been examined in cotton rats.

Materials and methods

Animals and specimen preparation

Animal experiments were performed in accordance with the guidelines of the Chitose Laboratory, Japan Food Research Laboratories (approval no. HK200703-01) and the Hokkaido Institute of Public Health (approval no. K30-01). Male animals of the following species were used in this study: C57BL/6NcrSlc mice at 3 months of age (Japan SLC, Shizuoka, Japan), HIS/Hiph cotton rats of various ages (maintained at Hokkaido Institute of Public Health), JclBrIHan:WIST rats at 2 months of age (CLEA Japan, Tokyo, Japan), and Kbl:JW rabbits at 6 to 12 months of age (Kitayama Labes, Nagano, Japan). The animals were euthanized with an intravenous injection of sodium pentobarbital in rabbits or by cutting the abdominal aorta under deep anesthesia with isoflurane in mice, cotton rats, and rats. After euthanasia, the femurs, tibiae, and caudal vertebrae were harvested, fixed with 10% neutral buffered formalin overnight to 7 days at room temperature. After removal of the soft tissue, the fixed bones were decalcified with 10% EDTA (pH 7.4, Muto Pure Chemicals, Tokyo, Japan), Morse's solution (pH 2.5, 10% sodium citrate and 20% formic acid, Fujifilm Wako Pure Chemical, Osaka, Japan), or K-CX solution (pH 0.2, 1.35 N HCl and chelator, Falma, Tokyo, Japan) (Noda et al. 2007). The endpoint of decalcification was identified when the microtome blade was inserted smoothly. Over-decalcification

Table 1 List of animal species and decalcification methods for bone specimens

Principle	Chelator	Organic acid	Inorganic acid	Over-decalcification
Decalcification				
Solution	10% EDTA2Na	Morse's solution	K-CX solution	K-CX solution
pH	7.0	2.5	0.2	0.2
Condition	2 to 12 weeks at RT	5 to 14 days at RT	1 to 3 days at 4 °C	4 to 5 days at RT
Animals, bones				
Mice, femurs	5	6	ne	ne
Cotton rats, caudal vertebrae	6	19	ne	ne
Rats, femurs	5	8	8	6
Rabbits, femurs and tibiae	7	10	10	6

For the cotton rats, caudal vertebrae on 0 day ($n=3$), 4 days ($n=3$), 7 days ($n=4$), 2 months ($n=3$), and 6 months ($n=6$) of age were fixed with 10% neutral buffered formalin and decalcified with Morse's solution

RT room temperature, ne not examined

was confirmed by the loss of nuclear staining with hematoxylin. The decalcified tissues were embedded in paraffin and cut into 4- μ m sections unless otherwise specified. Details of the bone samples are presented in Table 1.

Reagents

Weigert's iron hematoxylin, 1% Sirius red solution, saturated picric acid, 1% Alcian blue solution (pH 2.5), 0.4% aniline blue solution, 0.75% orange G solution, and solution of 2.5% phosphotungstic acid and 2.5% phosphomolybdic acid were purchased from Muto Pure Chemicals. Light green SF (Thermo Fisher Scientific, MA, USA), fast green FCF (Nacalai Tesque, Tokyo, Japan), and naphthol green B (Fuji-film Wako Pure Chemical) were also used. Picrosirius red (0.04%) was prepared by diluting 1% Sirius red solution with saturated picric acid. The dilutions of 0.5% picro-light green, 0.05% picro-fast green, and 1% picro-naphthol green were prepared by diluting 2% solution of each dye with saturated picric acid.

Picrosirius red for osteoid staining

For osteoid staining, deparaffinized sections were stained with 0.1% picrosirius red solution for 1 h at room temperature and washed with 1% acetic acid. For alcian blue/picrosirius red staining, deparaffinized sections were immersed in 3% acetic acid, stained with 1% alcian blue solution (pH 2.5) for 30 min at room temperature, and rinsed with 3% acetic acid. The sections were then stained with 0.1% or 0.04% picrosirius red for 5 min at room temperature and washed with 1% acetic acid. The sections were dehydrated, cleared, and mounted with a coverslip using an acrylic resin (EUKITT®, ORSAtec, Bobingen, Germany). The sections were observed using a BZ-X800 microscope (Keyence, Osaka, Japan) with attached polarized filters.

Selection of dyes for the mineralized bone

To examine suitable dyes for mineralized bone, we modified the Masson's trichrome staining protocol. Deparaffinized sections were stained with Weigert's iron hematoxylin for 10 min at room temperature and washed in tap water. The sections were then immersed in 2.5% phosphotungstic acid and 2.5% phosphomolybdic acid for 1 min at room temperature, rinsed with 1% acetic acid, followed by incubation in 0.75% orange G solution for 2 min at room temperature, and washed briefly in 1% acetic acid. Mineralized bone was stained with aniline blue, fast green FCF, light green SF, or naphthol green B solution in 1% acetic acid for 3 min at room temperature and rinsed with 1% acetic acid. The osteoid was stained with 0.04% picrosirius red solution for 5 min at room temperature and rinsed with 1% acetic acid. The sections were dehydrated, cleared, and mounted with a coverslip using an acrylic resin (EUKITT®, ORSAtec). To examine the effect of picric acid as a mordant, the mineralized bone was also stained with green dyes diluted with saturated picric acid, while 2.5% phosphotungstic acid and 2.5% phosphomolybdic treatment was omitted.

JFRL staining for osteochondral tissues and bone cells

The procedure of JFRL staining developed in this study is described as follows:

1. When staining for the cartilage, the sections were immersed in 3% acetic acid, then stained with 1% alcian blue solution (pH 2.5) for 20 min at room temperature, and rinsed with 3% acetic acid.
2. The sections were then stained with Weigert's iron hematoxylin for 10 min at room temperature and washed in tap water. The differentiation step with hydrochloric

acid can be omitted at this stage, because the dye can be differentiated by the saturated picric acid present in the subsequent steps.

- The sections were then stained in 0.75% orange G solution for 2 min at room temperature and washed briefly in 1% acetic acid.
- This was followed by staining the sections with 0.05% micro-fast green FCF, 0.5% micro-light green SF, or 1% micro-naphthol green for 3 min at room temperature and washed briefly in 1% acetic acid for staining of the mineralized bone. When co-staining for the cartilage, fast green FCF might be avoided due to its bluish color.
- The sections were stained with 0.04% picosirius red solution for 5–10 min at room temperature and washed in 1% acetic acid.
- The sections were finally dehydrated with graded alcohol, cleared with xylene, and mounted using an acrylic resin (EUKITT®, ORSAtec). The slides were immersed

in alcohol and xylene until the removal of excess picric acid to achieve a good color balance.

Results

Picosirius red for osteoid staining

First, we examined the staining methods which distinguish osteoid from mineralized bone, regardless of animal species and decalcification methods. As reported previously (Junqueira et al. 1986), picosirius red caused red birefringence in the osteoid portion and a weaker green to orange birefringence in mineralized bone under polarized light (Fig. 1a–d). The specificity of red birefringence in the osteoid was independent of both the animal species and decalcifying agents. Notably, osteoid-specific birefringence was maintained even in the over-decalcified specimen (Fig. 1d).

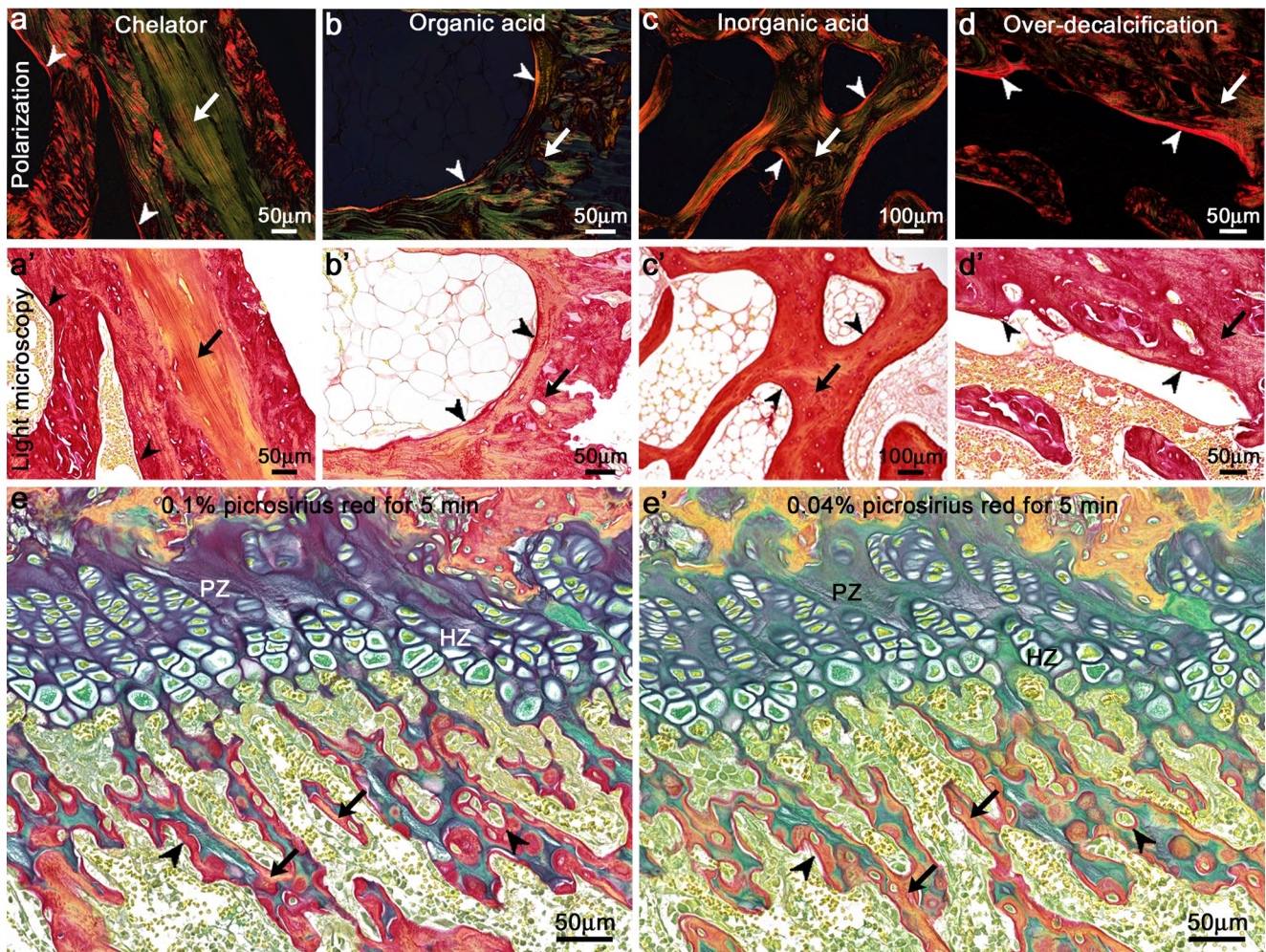


Fig. 1 Picosirius red staining for osteoid detection under both polarized microscopy and light microscopy. (**a–d**) Representative image of the (**a** and **a'**) rat femurs, (**b** and **b'**) caudal vertebrae of cotton rats, (**c** and **c'**) rabbit femurs, and (**d** and **d'**) rat femurs decalcified by indicated conditions. The sections were stained with 1% picosirius red for 1 h. (**e** and **e'**) Optimal conditions for osteoid staining by picosirius red under light microscopy. The rat femurs with over-decalcification were stained with 1% alcian blue (pH 2.5) followed by picosirius red of indicated conditions. Arrowheads: osteoid, arrows: mineralized bone, HZ: hypertrophic zone, PZ: proliferating zone

sius red for 1 h. (**e** and **e'**) Optimal conditions for osteoid staining by picosirius red under light microscopy. The rat femurs with over-decalcification were stained with 1% alcian blue (pH 2.5) followed by picosirius red of indicated conditions. Arrowheads: osteoid, arrows: mineralized bone, HZ: hypertrophic zone, PZ: proliferating zone

When the same stained sections were observed by light microscopy, 0.1% picosirius red for 1 h stained the bone as red, but it was not specific for the osteoid (Fig. 1a'–d'). In the over-decalcified specimen of the rat femur stained with 1% alcian blue (pH 2.5), using a shorter staining time of 5 min with 0.1% picosirius red increased the osteoid-specific red color compared to those sections stained for 1 h (Fig. 1 d' and e). However, the proliferating zone of the epiphyseal plate was stained blue and red with a color overlap (Fig. 1e). In contrast, co-staining of alcian blue and 0.04% picosirius red for 5 min stained the osteoid as red and the cartilage as blue with much less color overlap (Fig. 1e').

Identification of suitable dyes for staining the mineralized bone

We compared different dyes amongst the acidic dyes, with an aim to identify a suitable dye for the staining of mineralized bone. The different dyes compared were aniline blue, fast green FCF, light green SF, and naphthol green B. Rabbit femurs decalcified with inorganic acid were treated with 2.5% phosphotungstic acid and 2.5% phosphomolybdic acid as a

mordant. Aniline blue was more selective for the osteoid rather than mineralized bone, and the osteoid was stained blue and red with a color overlap (Fig. 2a–a''). In contrast, the other three dyes were more specific to mineralized bone, and the staining intensity was concentration-dependent (Fig. 2b–d''). Fast green FCF tended to stain the mineralized bone bluish in color than light green SF (Fig. 2 b–b'' and c–c''), while naphthol green B stained them as yellowish green with weaker staining intensity compared to light green SF (Fig. 2 c–c'' and d–d''). In addition, the combination of these green dyes and picosirius red clearly revealed the lamellar structure of green mineralized bone with repeated sequences of red lines (Fig. 2b–d''). The optimal concentration of these dyes was 0.05% in fast green FCF, 0.2 to 0.5% in light green SF, and 0.5 to 1% in naphthol green B.

Further, we also examined for a suitable specimen thickness and mordant for the combination of light green SF and picosirius red stains, and compared their staining specificity to picosirius red staining under polarized microscopy. At a specimen thickness of 2 or 4 μm , the mineralized bone was clearly distinguished from the osteoid with a clear mineralization front in both the woven and lamellar bone (Fig. 3 a and a'). Sections measuring more than 6 μm in thickness tended to increase the green intensity and overlap with the red color in the osteoid, especially in the

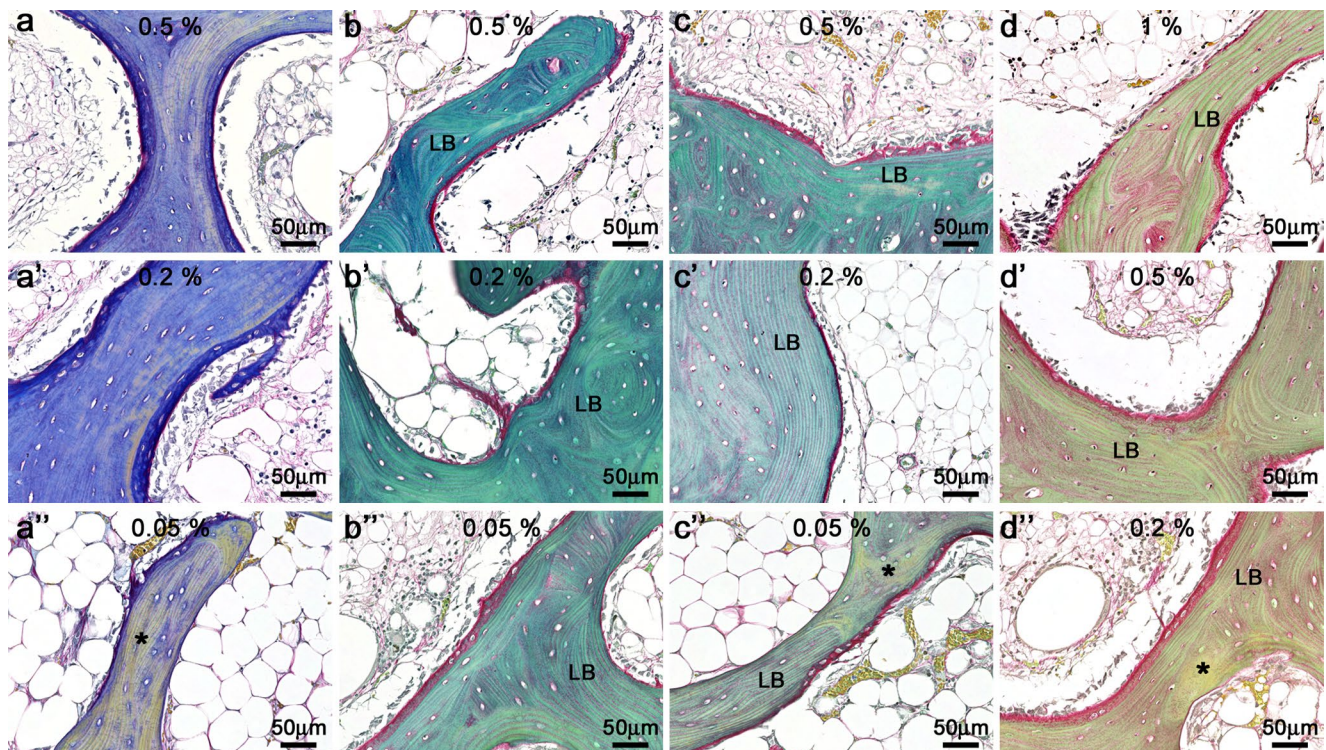


Fig. 2 Comparison of the dyes for staining of the mineralized bone combined with picosirius red. Representative image of the mineralized bone. The rabbit femurs decalcified with inorganic acid were stained with Weigert's iron hematoxylin, 0.75% orange G, followed by staining with (a–a'') aniline blue, (b–b'') fast green FCF, (c–c'')

light green SF, and (d–d'') naphthol green B of the indicated concentrations, and finally with 0.04% picosirius red. The sections were treated with 2.5% phosphomolybdic acid and 2.5% phosphotungstic acid as a mordant. Asterisks indicate the faint staining area of the mineralized bone. LB: lamellar bone

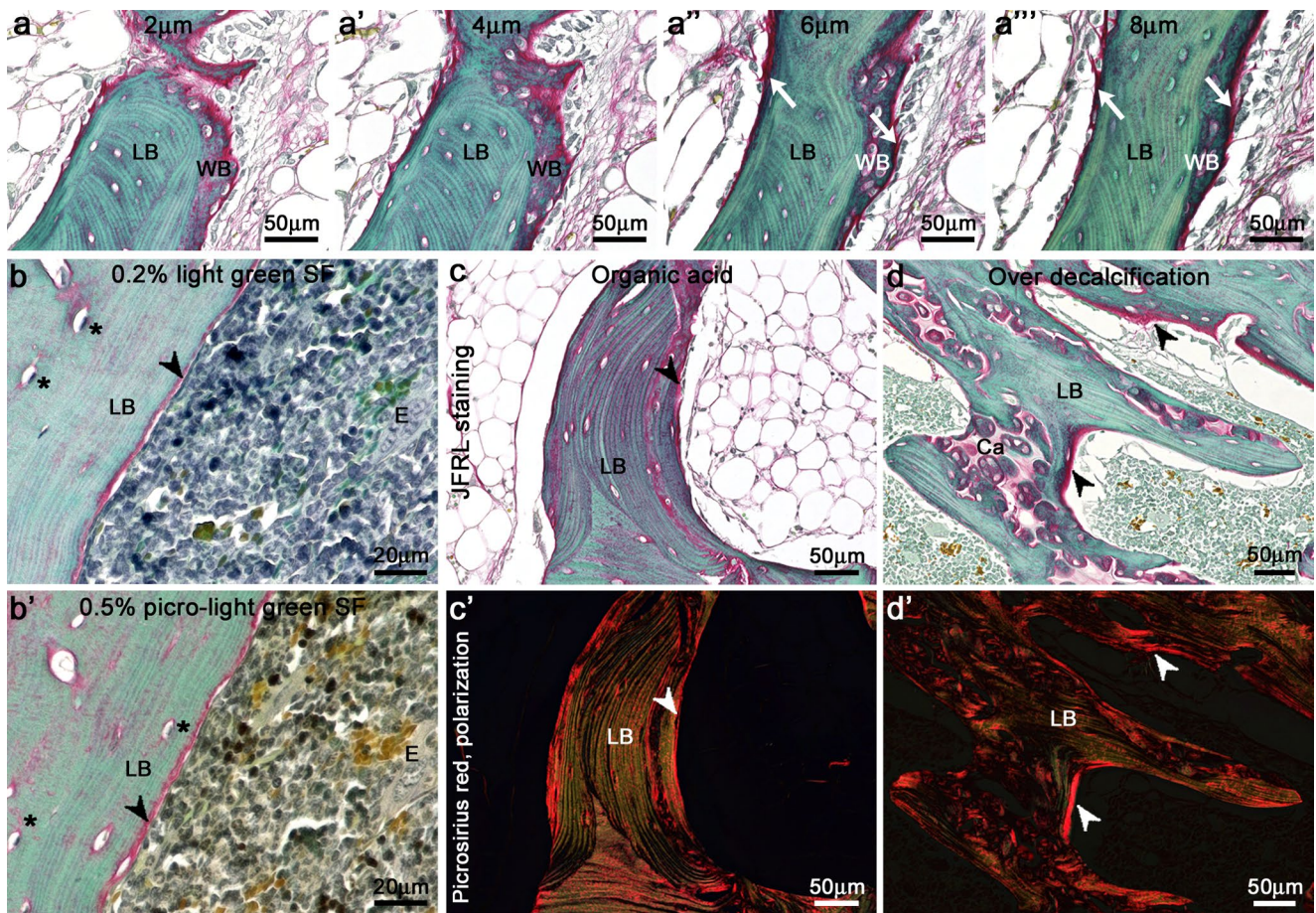


Fig. 3 Identifying a suitable specimen thickness and mordant for JFRL staining. (**a–a'''**) Specimen thickness suitable for the distinction of osteoid and mineralized bone. Serially sliced sections of rabbit femurs decalcified with inorganic agents are shown. (**b** and **b'**) Comparison of the mordants for JFRL staining. Sections of mice femurs decalcified with a chelator were treated with 2.5% phosphotungstic acid and 2.5% phosphomolybdic acid (upper panel) and

saturated picric acid (lower panel) as a mordant. (**c–d'**) Comparison of bone staining between JFRL staining and picrosirius red staining under light microscopy and polarized microscopy, respectively. Sections of rabbit femurs decalcified with organic acid and sections of over-decalcified rat femurs are shown. Arrows: the color overlap in mineralization front, arrowheads: osteoid, asterisks: osteocytes, Ca: cartilage, E: erythrocytes, LB: lamellar bone, WB: woven bone

mineralization front (Fig. 3 a'' and a'''). When solution of 2.5% phosphotungstic acid and 2.5% phosphomolybdic acid was used as a mordant, 0.2% light green SF tended to stain red blood cells which were already stained with Orange G as green (Fig. 3b). Notably, 0.5% picro-light green SF kept erythrocytes orange and stained the mineralized bone more greenish without decreasing staining intensity (Fig. 3b'). With either mordant, oval osteocytes were found in the lacunae of mineralized bone (Fig. 3 b and b'). The specificity of osteoid by picrosirius red and mineralized bone by light green SF was identical to picrosirius red staining under polarizing microscopy (Fig. 3c–d').

Visualization of osteochondral tissue and bone cells by JFRL staining

The cartilage was not stained with either light green SF or picrosirius red stains (Fig. 3d). Therefore, we stained the

cartilage with 1% alcian blue (pH 2.5) and the osteoid with picrosirius red combined with 0.05% picro-fast green FCF, 0.5% picro-light green SF, and 1% picro-naphthol green B to observe endochondral ossification. The rat femurs decalcified with organic acid or over-decalcified ones were used. Because picro-fast green FCF colored the mineralized bone and hyaline cartilage as bluish green, the mineralized bone was less indistinguishable from the hyaline cartilage (Fig. 4 a and a'). Picro-light green SF (Fig. 4b) and picro-naphthol green B (Fig. 4c) distinguished the hyaline cartilage, osteoid, and mineralized bone by distinctly different colors (blue, red, and green, respectively) in the sections decalcified with organic acid. The mineralized bone was stained weaker and more yellowish with picro-naphthol green B compared with picro-light green SF staining (Fig. 4 b and c). In the rat femur with over-decalcification, although the proliferating zone of the epiphyseal plate was slightly co-stained with

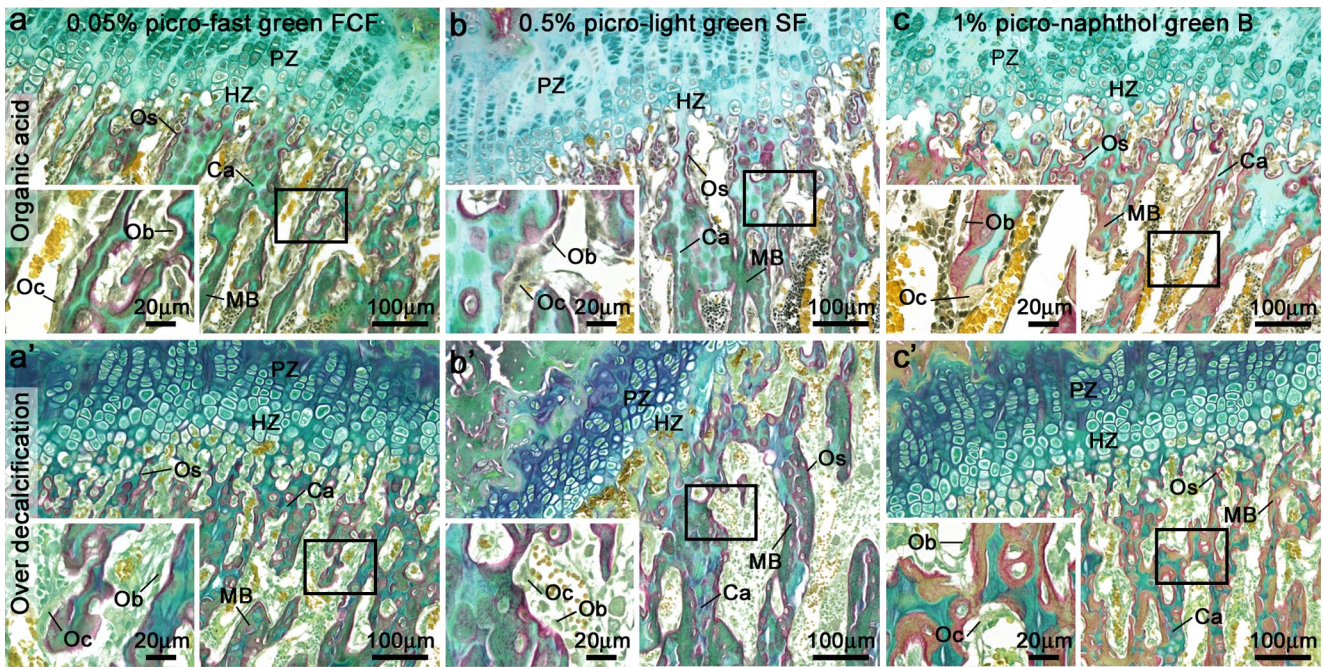


Fig. 4 Simultaneous detection of osteochondral matrix and bone cells in endochondral ossification. Endochondral ossification of the rat femur (a–c) decalcified with organic acid or (a’–c’) those with over-decalcification. Representative images of JFRL staining using (a and a’) 0.05% picro-fast green FCF, (b and b’) 0.5% picro-light green SF,

or (c and c’) 1% picro-naphthol green B are shown. The black box is magnified in the lower-left panel. Ca: cartilage of the trabeculae, HZ: hypertrophic zone, MB: mineralized bone, Ob: osteoblasts, Oc: osteoclasts, Os: osteoid, PZ: proliferating zone

red and blue, the hyaline cartilage, osteoid, and mineralized bone were all easily distinguishable (Fig. 4 b’ and c’). In the sections decalcified with organic acid, osteoblasts and osteoclasts were easily identified. The former was lined along the osteoid and had blackish cytoplasm, and the latter had large

and greenish cytoplasm and multiple nuclei (Fig. 4a–c). In the over-decalcified sections, the osteochondral tissue was easily distinguished, although the nuclei were not stained, and osteoblasts and osteoclasts were less easily identified (Fig. 4 b’ and c’).

Table 2 Summary of staining characteristics by JFRL staining

Structure	Color	Corresponding dyes
Cartilage matrix		
Hyaline cartilage	Blue to purple	Alcian blue
Fibrocartilage	Blue, green, and red	Alcian blue, light green SF, sirius red
Bone matrix		
Osteoid	Red	Sirius red
Mineralized bone	Green	Light green SF
Lamellar bone	Green with repeated sequences of red line	Light green SF, sirius red
Woven bone	Green with various degrees of red patches	Light green SF, sirius red
Cells		
Osteoblasts	Single nucleus with blackish cytoplasm	Weigert’s iron hematoxylin
Osteocytes	Single nucleus with oval shape	Weigert’s iron hematoxylin
Osteoclasts	Multiple nuclei with greenish cytoplasm	Weigert’s iron hematoxylin, light green SF
Erythrocytes	Yellow to orange	Orange G
Cell nuclei	Black to dark brown	Weigert’s iron hematoxylin
Cytoplasm	Various colors	Weigert’s iron hematoxylin, light green SF

The color of the cartilage matrix depends on the age and decalcification conditions. The green of the mineralized bone varies from yellowish green to bluish green depending on the dye and solvent used

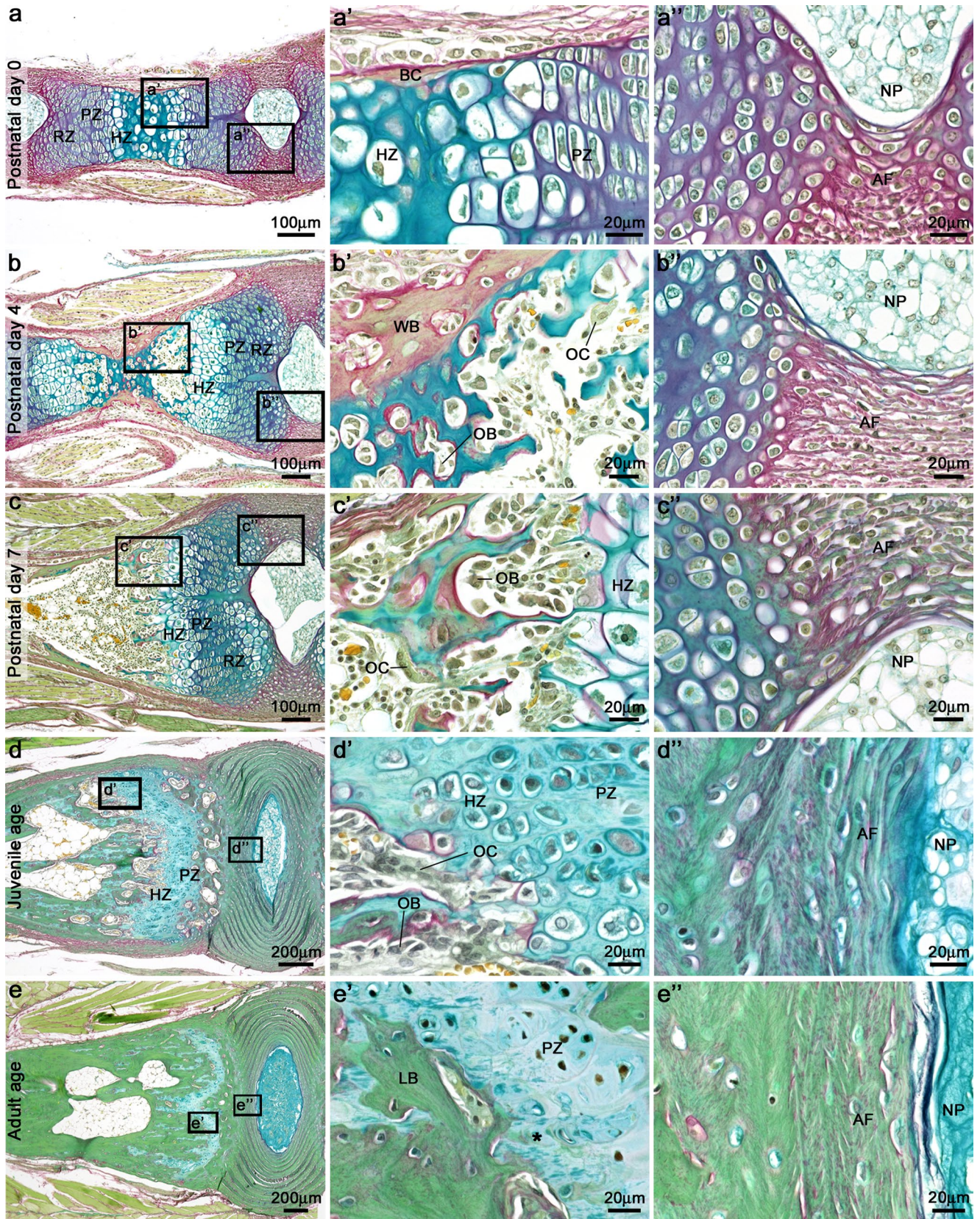


Fig. 5 Age-related changes in the caudal vertebrae of cotton rats. (a–e) Longitudinal sections of the caudal vertebrae of cotton rats decalcified with organic acid. Black boxes are magnified in the next panel showing the (a'–e') hyaline cartilage and (a''–e'') fibrocartilage. Asterisk indicates bone formation within the epiphyseal plate. AF: annulus fibrosus, BC: bone collar, HZ: hypertrophic zone, LB: lamellar bone, NP: nucleus pulposus, Ob: osteoblasts, Oc: osteoclasts, Os: osteoid, PZ: proliferating zone, RZ: resting zone, WB: woven bone

The overall staining characteristics of JFRL staining are summarized in Table 2. This novel polychrome method stained the cartilage as blue by alcian blue, osteoid as red by Sirius red, and the mineralized bone as green depending on the dye (Figs. 3 and 4). The nuclei were revealed as black, the cytoplasm as various colors, and red blood cells as orange (Figs. 3 and 4). Osteoblasts and osteoclasts can be distinguished by their cell shape; however, the nuclei were not stained in the over-decalcified sections (Fig. 4). Osteocytes had oval shape and were localized in the lacunae of mineralized bone (Fig. 3 b and b').

Time-course changes in the caudal vertebrae of cotton rats showing tail autotomy

Using JFRL staining, we examined the time-course changes in the caudal vertebrae of cotton rats (*Sigmodon hispidus*), which has a relatively shorter tail and shows false caudal autotomy (Faith et al. 1997; Hosotani et al. 2021). On postnatal day 0, the caudal vertebrae were composed of hyaline cartilage, which was observed as purple in their epiphyseal and blue in their diaphysis, and the periphery of the diaphysis was surrounded by bone collar stained red and green (Fig. 5 a and a'). On postnatal day 4, the hyaline cartilage of the diaphysis was replaced by mineralized bone and bone marrow with cartilage absorption by osteoclasts and osteoid secretion by osteoblasts (Fig. 5 b and b'). The bone collar became thicker, forming woven bone characterized by green and red matrix with irregular arrangement of osteoid and osteocytes (Fig. 5b'). On postnatal day 7, the hyaline cartilage was almost replaced by the bone matrix and bone marrow at the diaphysis (Fig. 5c), and primary trabeculae were slightly produced (Fig. 5c'). At the juvenile age, the epiphyseal plate became obvious, and primary trabeculae extended toward the diaphysis (Fig. 5 d and d'). In contrast, the epiphyseal plate became thinner and the hypertrophic zone was absent at the adult age (Fig. 5 e and e'). A large region of the cartilage did not contain chondrocytes, and the remaining cells were small (Fig. 5e'). Lamellar bone extending horizontally to the epiphyseal plate and small bone formation was also found within the epiphyseal plate (Fig. 5e'). The fibrocartilage consisting of the annulus fibrosus at the epiphyseal region was stained purple at postnatal day 0, which became greenish with aging and was stained mainly green in juvenile age and thereafter (Fig. 5a''–e'').

Discussion

In this study, we developed a novel staining method called JFRL staining, which distinguishes the osteochondral matrix and identifies bone cells. We also identified the staining dyes and concentrations which were not affected by the decalcifying conditions and examined the staining protocol for robustness and high reproducibility. The final procedure for JFRL staining is summarized in Supplemental Table 1.

This study demonstrated that the osteoid-specific birefringence by picrosirius red was independent of decalcifying conditions, as observed even in over-decalcified sections under polarized microscopy. Picrosirius red, which is a Sirius red solution diluted in saturated picric acid, visualizes the osteoid as red birefringence under polarized microscopy (Junqueira et al. 1979, 1986). Sirius red specifically binds to the [Gly-x-y] triple-helix structure in all collagen fibers and is used for the quantitative detection of all types of collagen in histology and biochemistry (Kliment et al. 2011; Segnani et al. 2015). Osteoid and mineralized bone contain 90% and 30% of type I collagen, respectively (Rosset and Bradshaw 2016). It was previously shown that collagen fibrils do not degrade after decalcification (Fujita and Fujita 2002). Therefore, the amount of collagen and preservation of their structures during decalcification might be the reason for the distinguishing of the osteoid from the calcified bone by picrosirius red dye. In addition, a lower concentration and shorter staining time of picrosirius red increased the staining specificity of the osteoid under light microscopy. Consistent with this, picrosirius red is routinely used at a concentration of 0.1% for polarized observation and at approximately 0.04% for light microscopy, similar to other methods such as Sirius red/fast green and elastica van Gieson staining (Junqueira et al. 1986; Segnani et al. 2015; Tomida et al. 2019). Taken together, these results highlight that picrosirius red is suitable for osteoid staining under both polarized and light microscopy, regardless of decalcification conditions.

Since both calcified and osteoid bone contain type I collagen (Rosset and Bradshaw 2016), we chose a dye compatible with calcified bone from the dyes—light green SF, fast green FCF, and naphthol green B, commonly used for collagen staining. The results indeed showed that the calcified bone is stained green similar to that in Masson–Goldner staining and Villanueva–Goldner staining, which uses light green SF and naphthol green B, respectively (Junqueira et al. 1986; Rentsch et al. 2014; Nakata et al. 2016). By using saturated picric acid as a mordant, mineralized bones were stained more yellowish compared to staining seen when using 2.5% phosphotungstic acid and 2.5% phosphomolybdic acid as a mordant. In addition, picric acid retained the orange stain in erythrocytes as stained by Orange G. Since fast green FCF stained the mineralized bone as bluish green regardless of

mordants, we argue that this dye might be less suitable for co-staining the calcified bone and cartilage. Taken together, it can be concluded that picro-light green SF is the most suitable dye for staining mineralized bone while simultaneously staining the cartilage, osteoid, and calcified bone, all in one section, although we found that picro-naphthol green B might also be useful.

Since the present study indicated that the novel staining we developed distinguished osteoid and mineralized bone by the collagen content, we named it Join of the Five dyes Revealing collagenous tissue (JFRL) staining. Notably, JFRL staining also distinguishes between lamellar bone and woven bone, and among osteoblasts, osteocytes, and osteoclasts regardless of decalcification conditions and experimental animal species examined. Recently, a trichrome staining was reported for musculoskeletal tissues using picosirius red, fast green FCF, and alcian blue, which also differentiates osteoid and mineralized bone as red and green, respectively (Gaytan et al. 2020). However, unlike JFRL staining, both osteoid and the interterritorial matrix of hyaline cartilage were stained red, and the staining did not use iron hematoxylin and orange G for staining of the cellular components. Therefore, JFRL staining might be a more suitable method for osteochondral tissue, especially at the interface of osteocartilage.

To verify the usefulness of JFRL staining, we used the caudal vertebrae of cotton rats as a specimen for observing the histomorphology using JFRL staining. Cotton rats have unique phenotypes in their tail, that is, a shorter tail and false caudal autotomy characterized by loss of the tail sheath along the fracture plane with the caudal vertebrae remaining (Faith et al. 1997; Hosotani et al. 2021). Although the fracture plane of the skin has been clarified, those of the caudal vertebrae have not yet been examined in cotton rats. In addition, the histological characteristics of the shorter tail have not been identified until now. In the neonatal cotton rats, the caudal vertebrae were developed by endochondral ossification to form mineralized bone by osteoblasts and osteoclasts. At juvenile age of the cotton rats, the epiphyseal plates of caudal vertebrae had many chondrocytes and were replaced by spongy bone along longitudinal rows. In contrast, the South American rodent *Proechimys cuvieri* has a large area and loose structure of the epiphyseal plate, which functions as a fracture surface (Dubost and Gasc 1987). Therefore, it is hypothesized that cotton rats develop false caudal autotomy due to normal development of the caudal vertebrae without a fracture plane. In cotton rats at an adult age (6 months), which is much less than the lifespan of captive-bred cotton rats (usually 23 months) (Faith et al. 1997), the number of chondrocytes declined and the hypertrophic zone was absent at the epiphyseal plate. In addition, bones were formed parallel to the epiphyseal plate and within the epiphyseal plate. These changes are also observed in the long bones of rats

that have reached their lifespan (Roach et al. 2003). This observation indicates that the longitudinal extension of the caudal vertebra is lost at a younger age, which might reflect the shorter tail in the cotton rats. As described above, JFRL staining unveiled histological characteristics of the bone regarding caudal false autotomy and a shorter tail, and has been shown to be useful for examining bone physiology.

In conclusion, JFRL staining, to the best of our knowledge, is the first method to simultaneously distinguish cartilage, osteoid, and calcified bone, regardless of decalcification conditions and animal species. This method also distinguishes between lamellar bone and woven bone, and among osteoblasts, osteocytes, and osteoclasts. The novel JFRL staining will provide new information in a wide range of biomedical fields, including bone development, physiology, and pathology. Although the current study showed that JFRL staining is not dependent on the experimental animal species examined, further studies using both normal bones and bone lesions in a wider range of animal species, including humans, are required to further verify the robustness of this staining.

Supplementary Information The online version contains supplementary material available at <https://doi.org/10.1007/s00441-021-03516-6>.

Author contribution Conception of the work: TN, OI, KN, YK, TM, TY. Design of the work: TN, OI, KN, YK, TM. Acquisition of data for the work: TN, KS, ET, MH, TN, TI. Analysis of data for the work: TN, KS, ET, MH, TN. Interpretation of data for the work: TN, KS, ET, TN, OI, YK, TM, TY. All authors have revised the manuscript, approved the final manuscript, and agreed to account for all aspects of the work.

Funding This study was funded by JSPS KAKENHI (Grant Number: JP18K0703708).

Declarations

Ethics approval Animal experiments were performed in accordance with the guidelines of the Chitose Laboratory, Japan Food Research Laboratories (approval no. HK200703-01) and the Hokkaido Institute of Public Health (approval no. K30-01).

Conflict of interest The authors declare no competing interests.

References

- Bahney CS, Zondervan RL, Allison P et al (2019) Cellular biology of fracture healing. *J Orthop Res* 37:35–50. <https://doi.org/10.1002/jor.24170>
- Bogoevski K, Woloszyk A, Blackwood K et al (2019) Tissue morphology and antigenicity in mouse and rat tibia: comparing 12 different decalcification conditions. *J Histochem Cytochem* 67:545–561. <https://doi.org/10.1369/0022155419850099>
- Dubost G, Gasc JP (1987) The process of total tail autotomy in the South-American rodent, *Proechimys*. *Journal of Zoology* 212(3):563–572. <https://doi.org/10.1111/j.1469-7998.1987.tb02924.x>

- Faith RE, Montgomery CA, Durfee WJ et al (1997) The cotton rat in biomedical research. *Lab Anim Sci* 47:337–345
- Fujita H, Fujita T (2002) Textbook of histology Part 1, 4th edn. Igaku-Shoin, Tokyo, pp 186 (in Japanese)
- Gaytan F, Morales C, Reymundo C, Tena-Sempere M (2020) A novel RGB-trichrome staining method for routine histological analysis of musculoskeletal tissues. *Sci Rep* 10:16659. <https://doi.org/10.1038/s41598-020-74031-x>
- Gilbert SF (2000) Osteogenesis: the development of bones. In: *Developmental biology*, 6th edn. Sinauer Associates, Sunderland (MA). <https://www.ncbi.nlm.nih.gov/books/NBK10056/>
- Hosotani M, Nakamura T, Ichii O et al (2021) Unique histological features of the tail skin of cotton rat (*Sigmodon hispidus*) related to caudal autotomy. *Biol Open* 10:bio058230. <https://doi.org/10.1242/bio.058230>
- Junqueira LC, Assis Figueiredo MT, Torloni H, Montes GS (1986) Differential histologic diagnosis of osteoid. A study on human osteosarcoma collagen by the histochemical picosirius-polarization method. *J Pathol* 148:189–196. <https://doi.org/10.1002/path.1711480210>
- Junqueira LC, Bignolas G, Brentani RR (1979) Picosirius staining plus polarization microscopy, a specific method for collagen detection in tissue sections. *Histochem J* 11:447–455. <https://doi.org/10.1007/BF01002772>
- Kliment CR, Englert JM, Crum LP, Oury TD (2011) A novel method for accurate collagen and biochemical assessment of pulmonary tissue utilizing one animal. *Int J Clin Exp Pathol* 4:349–355
- Kulak CA, Dempster DW (2010) Bone histomorphometry: a concise review for endocrinologists and clinicians. *Arq Bras Endocrinol Metab* 54:87–98. <https://doi.org/10.1590/s0004-27302010000200002>
- Moreira CA, Dempster DW, Baron R (2019) Anatomy and ultrastructure of bone – histogenesis, growth and remodeling mdtext.com. In: *Endotext* [Internet]. South Dartmouth (MA). <https://www.ncbi.nlm.nih.gov/books/NBK279149/>
- Nakata H, Kuroda S, Tachikawa N et al (2016) Histological and micro-computed tomographic observations after maxillary sinus augmentation with porous hydroxyapatite alloplasts: a clinical case series. *Springerplus* 5:260. <https://doi.org/10.1186/s40064-016-1885-2>
- Niewiesk S, Prince G (2002) Diversifying animal models: the use of hispid cotton rats (*Sigmodon hispidus*) in infectious diseases. *Lab Anim* 36:357–372. <https://doi.org/10.1258/002367702320389026>
- Noda K, Nakamura Y, Oikawa T et al (2007) A new idea and method of tooth movement using a ratchet bracket. *Eur J Orthod* 29:225–231. <https://doi.org/10.1093/ejo/cjm002>
- Ralis ZA, Watkins G (1992) Modified tetrachrome method for osteoid and defectively mineralized bone in paraffin sections. *Biotech Histochem* 67:339–345. <https://doi.org/10.3109/10520299209110046>
- Rentsch C, Schneiders W, Manthey S et al (2014) Comprehensive histological evaluation of bone implants. *Biomater* 4:e27993. <https://doi.org/10.4161/biom.27993>
- Roach HI, Mehta G, Oreffo RO et al (2003) Temporal analysis of rat growth plates: cessation of growth with age despite presence of a physis. *J Histochem Cytochem* 51:373–383. <https://doi.org/10.1177/002215540305100312>
- Rosset EM, Bradshaw AD (2016) SPARC/osteonectin in mineralized tissue. *Matrix Biol* 52–54:78–87. <https://doi.org/10.1016/j.matbio.2016.02.001>
- Segnani C, Ippolito C, Antonioli L et al (2015) Histochemical detection of collagen fibers by Sirius red/fast green is more sensitive than van Gieson or Sirius red alone in normal and inflamed rat colon. *PLoS ONE* 10:e0144630. <https://doi.org/10.1371/journal.pone.0144630>
- Tomida S, Aizawa K, Nishida N et al (2019) Indomethacin reduces rates of aortic dissection and rupture of the abdominal aorta by inhibiting monocyte/macrophage accumulation in a murine model. *Sci Rep* 9:10751. <https://doi.org/10.1038/s41598-019-46673-z>
- Ueno T (1985) Comparative study of various methods for identification of osteoid matrix in decalcified bone. *Jpn J Oral Biol* 27:495–508. <https://doi.org/10.2330/joralbiosci1965.27.495>
- Yoshiki S (1973) A simple histological method for identification of osteoid matrix in decalcified bone. *Stain Technol* 48:233–238. <https://doi.org/10.3109/10520297309116630>

Publisher's Note Springer Nature remains neutral with regard to jurisdictional claims in published maps and institutional affiliations.